A survey of Rashba and Dresselhaus effects in hybrid organic-inorganic perovskites

Mikaël Kepenekian,[1,*] Roberto Robles,[2] Claudine Katan,[1]
Daniel Sapori,[3] Laurent Pedesseau,[3] and Jacky Even[3,†]

[1]*Institut des Sciences Chimiques de Rennes,*
UMR 6226, CNRS - Université de Rennes 1, France
[2]*ICN2 - Institut Catala de Nanociencia i Nanotecnologia,*
Campus UAB, 08193 Bellaterra (Barcelona), Spain
[3]*Université Européenne de Bretagne, INSA,*
FOTON UMR 6082, 35708 Rennes, France

(Dated: July 14, 2015)

Abstract

We use symmetry analysis, density functional calculations and $k \cdot p$ modeling to scrutinize Rashba and Dresselhaus effects in hybrid organic-inorganic halide perovskites. This class of perovskites currently acts as the superstar of photovoltaic technology. Due to a large spin-orbit coupling, it also demonstrates great potential for spin-based applications. With a detailed study of the electronic structures and bulk lattice symmetries of a variety of systems, we detail the origin of the spin splitting in two-and three-dimensional hybrid perovskites. Finally, we show that low-dimensional nanostructures of $CH_3NH_3PbX_3$ (X=I, Br) lead to splittings that can be controlled by an applied electric eld. This new demonstration further opens the door to a perovskite-based spintronics.

INTRODUCTION

Ever since 2009 and the pioneer work of Miyasaka and coworkers[1] 3-dimensional (3D) solution-processed hybrid organic-inorganic halide perovskites AMX_3 (where A is an organic cation, M is Pb, Sn or Ge and X is I, Br or Cl) have attracted increasing attention from the photovoltaic community. Such a craze arises from the early successes met in improving the efficiency in the solar-to-electricity conversion combined with low costs of production.[2–4] As a result of these intense efforts, the efficiency records went from 3.8%[1] up to 20.1%[5] in only five years. Prior to the solar cell intense activity, hybrid halide perovskites were most popular in the 2-dimensional (2D), *i.e.* layered, form as they have shown good potential for applications in optoelectronics and microelectronics.[6–8] The wide range of applications available for these materials is a result of the impressive diversity of structures that can be obtained by varying the organic cation, the metal or the halide.

Although perovskites have been studied for decades, it is only recently that the major role of spin-orbit coupling (SOC) has been underlined by calculations based on density functional theory (DFT).[9–11] In addition to an improved description of the band structures and optoelectronic properties, it has led to the prediction of Rashba and/or Dresselhaus spin splitting in those hybrid systems. Dresselhaus[12] and Rashba[13] effects correspond originally to spin-splittings in zinc-blende and würtzite structures, respectively. Later, Bychkov and Rashba pointed out that the Rashba term occurs also in quasi-2D systems.[14] These effects have been extensively studied[15–19] and have been observed in various systems such as heterostructures,[20,21] quantum wells (QWs),[22–25] bulks,[26,27] heavy atoms and alloys surfaces,[16,28–35] or nanowires (NWs).[36–38] Eventually, the control of spin-dependent band structure provide with the opportunity to manipulate the spin with potential applications in spintronics.[39–42] In the case of hybrid halide perovskites, a Rashba spin splitting has been predicted in methylammonium-based perovskites $CH_3NH_3MX_3$ (M = Pb, Sn and X = I, Br),[11,43,44] and in formamidinium tin iodide $NH_2CHNH_2SnI_3$.[45] A hybrid halide perovskite-based spintronics is also supported by recent experimental studies on ferroelectric domains in thin films[46] and on the spin dynamics in $CH_3NH_3PbI_3$ that determined a spin relaxation lifetime around 7 ps.[47]

In this letter, we conduct a survey over two- and three-dimensional hybrid halide perovskites. On the basis of symmetry analysis and DFT calculations we discuss the possibility

of designing spintronic devices based on these materials. We start by recalling general features of Rashba and Dresselhaus spin-splittings. We focus then on systems presenting a non-centrosymmetric group space. Those exhibits naturally a Rashba or Dresselhaus splitting. Finally, we show that centrosymmetric system can present a tunable splitting through external electric field. The latter result opens the way for perovskite-based spintronics applications.

SPIN-ORBIT COUPLING AND SYMMETRY POINT GROUPS: RASHBA AND DRESSELHAUS SPIN SPLITTINGS

In the presence of SOC, we consider the following Hamiltonian

$$\mathcal{H} = \frac{\mathbf{p}^2}{2m} + V + \mathcal{H}_{SO},$$

where V is the lattice periodic crystal potential and $\mathcal{H}_{SO}$ the spin-orbit interaction term

$$\mathcal{H}_{SO} = \frac{\hbar}{4m^2c^2} \left(\nabla V \times \mathbf{p}\right) \cdot \sigma,$$

where $\hbar$ is Planck's constant, m the mass of an electron, c the velocity of light, $\mathbf{p}$ the momentum operator and $\sigma = (\sigma_x, \sigma_y, \sigma_z)$ the vector of Pauli spin matrices. Starting from a Bloch states description $\psi_{n\mathbf{k}}$

$$\psi_{n\mathbf{k}}(\mathbf{r}) = e^{i\mathbf{k}\cdot\mathbf{r}} \phi_{n\mathbf{k}}(\mathbf{r}),$$

the eigenvalue problem for $\phi_{n\mathbf{k}}$ reads

$$\left(\mathcal{H}^0(\mathbf{k}) + \mathcal{H}_{SO}(\mathbf{k})\right) \phi_{n\mathbf{k}}(\mathbf{r}) = \epsilon_n(\mathbf{k}) \phi_{n\mathbf{k}}(\mathbf{r}),$$

with

$$\mathcal{H}^0(\mathbf{k}) = \frac{(\hbar\mathbf{k} + \mathbf{p}^2)}{2m} + V$$
$$\mathcal{H}_{SO}(\mathbf{k}) = \frac{\hbar}{4m^2c^2} \left(\nabla V \times (\hbar\mathbf{k} + \mathbf{p}) \cdot \sigma\right)$$

It is common to treat SOC as a perturbation of the $\mathcal{H}^0$ zero-order Hamiltonian, which is solved following the $\mathbf{k} \cdot \mathbf{p}$ expansion around a given $\mathbf{k}_0$ leading to $\phi^0_{n\mathbf{k}}$ solution of the unperturbed Hamiltonian with the eigenvalue $\epsilon^0_n(\mathbf{k})$. It is completed by a spin function ω_s ($s = \pm 1/2$), keeping $\phi^0_{n\mathbf{k}s} = \phi^0_{n\mathbf{k}}\omega_s$ an eigenvector of $\mathcal{H}^0(\mathbf{k})$. We will note $\phi^0_{n\mathbf{k}\uparrow}$, $\phi^0_{n\mathbf{k}\downarrow}$ the spinors and $\epsilon^0_{n\uparrow}(\mathbf{k})$, $\epsilon^0_{n\downarrow}(\mathbf{k})$ the corresponding eigenvalues for $s = +1/2$ and $-1/2$, respectively.

The time reversal symmetry is conserved by SOC and delivers general conditions for conjugated spinors (Kramers' degeneracy)

$$\epsilon^0_{n\uparrow}(\mathbf{k}) = \epsilon^0_{n\downarrow}(-\mathbf{k}) \text{ and } \epsilon^0_{n\downarrow}(\mathbf{k}) = \epsilon^0_{n\uparrow}(-\mathbf{k})$$

Inversion symmetry yields additional conditions

$$\epsilon^0_{n\uparrow}(\mathbf{k}) = \epsilon^0_{n\uparrow}(-\mathbf{k}) \text{ and } \epsilon^0_{n\downarrow}(\mathbf{k}) = \epsilon^0_{n\downarrow}(-\mathbf{k})$$

Combining both symmetries leads to a double spin degeneracy

$$\epsilon^0_{n\uparrow}(\mathbf{k}) = \epsilon^0_{n\downarrow}(\mathbf{k})$$

across all the dispersion diagram within the Brillouin zone (BZ). When inversion symmetry is lost, the later spin degeneracy condition can be lost for a general wave vector, except for special high symmetry points leading to a band splitting.[11,48]

We take for $\mathbf{k}_0$ a special symmetry point of the BZ for which the spin degeneracy is conserved. The in-plane wave vector $\mathbf{k}_{||}$ is naturally defined for a 2D electron gas. In a 3D system, it belongs to the plane normal to a high symmetry axis, defining $\mathbf{k}_\perp$. Then one can apply the quasi-degenerate perturbation theory with the perturbative Hamiltonian *i.e.* the Rashba Hamiltonian[15]

$$\mathcal{H}_R = \alpha(\mathbf{k}) \cdot \sigma \tag{1}$$

with

$$\alpha(\mathbf{k}) = \langle \phi_{n\mathbf{k}} | \frac{\hbar}{4m^2c^2} \left(\nabla V \times (\hbar\mathbf{k} + \mathbf{p}) \right) | \phi_{n\mathbf{k}} \rangle.$$

Then one can take advantage of the symmetry to sort terms and identify the vanishing ones. The polynomial form of α has been previously derived in different works.[15,17,49] Clearly, due to time reversal symmetry, only odd power terms are relevant in the development. Vajna and coworkers[49] have precisely described how to determine the linear and cubic terms of $\mathcal{H}_R$ thanks to irreducible representations of relevant point groups for C_n and C_{nv} (n = 2, 3, 4). It has been recently completed for D_{2d} point groups.[17]

Let us illustrate these results with the example of a quasi-2D system in C_{2v} symmetry. Limiting the expansion to linear terms, only four contributions are to be considered: $k_x\sigma_y$, $k_y\sigma_x$, $k_x\sigma_x$ and $k_y\sigma_y$. It leads to the Rashba-Dresselhaus Hamiltonian:

$$H_{RD}(\mathbf{k}_{||}) = \lambda_R(k_x\sigma_y - k_y\sigma_x) + \lambda_D(k_x\sigma_x - k_y\sigma_y), \tag{2}$$

where $\mathbf{k}_{||} = (\mathbf{k}_x, \mathbf{k}_y)$ and $\mathbf{k}_\perp = \mathbf{k}_z$. For $\lambda_D = 0$, we retrieve the pure Rashba effect (a.k.a. Bychkov-Rashba effect) that trace back to Site Inversion Asymmetry (SIA) found in classical semiconductor quantum structures.[15] For $\lambda_R = 0$, the remaining term is found commonly in zinc blende structures and related to the so-called Bulk Inversion Asymmetry (BIA),[15] it is labelled here as the Dresselhaus effect. The solution of the eigenvalue problem give us the dispersion relation for the upper (E_{RD+}) and lower (E_{RD-}) branches away from $\mathbf{k_0}$, as well as the corresponding eigenvectors:

$$E_{RD\pm}(\mathbf{k}_{||}) = \frac{\hbar k_{||}^2}{2m} \pm \sqrt{(\lambda_D^2 + \lambda_R^2)(k_x^2 + k_y^2) - 4\lambda_D \lambda_R k_x k_y} \tag{3}$$

$$\Psi_{RD\pm}(\mathbf{k}_{||}) = \frac{e^{i\mathbf{k}_{||}\cdot\mathbf{r}}}{2\pi\hbar}\frac{1}{\sqrt{2}} \begin{pmatrix} \mp\dfrac{-\lambda_D(k_x + ik_y) + i\lambda_R(k_x - ik_y)}{\sqrt{(\lambda_D^2 + \lambda_R^2)(k_x^2 + k_y^2) - 4\lambda_D\lambda_R k_x k_y}} \\ 1 \end{pmatrix} \tag{4}$$

If $\lambda_D = 0$, then the energetic splitting $\Delta E_R = E_{R+} - E_{R-}$ is given by

$$\Delta E_R(\mathbf{k}_{||}) = 2\lambda_R\sqrt{k_x^2 + k_y^2}. \tag{5}$$

The same relation exist with λ_D if λ_R is null. Then, λ the non-null coefficient in both limit cases, is given by the band splitting away from the high symmetry point by

$$\lambda = \frac{\Delta E(\mathbf{k}_{||})}{2\sqrt{k_x^2 + k_y^2}}, \tag{6}$$

with $\Delta E = E_+ - E_-$ (Figure 1-a). In mixed cases, the band splitting alone cannot discriminate the relative strength of Rashba and Dresselhaus effects. One has to turn to the expectation value of the Pauli operator $\langle\sigma\rangle_{RD\pm} = \langle\Psi_{RD\pm}|\sigma|\Psi_{RD\pm}\rangle$.

It is convenient to write $\mathbf{k}_{||} = k_{||}(\cos\theta, \sin\theta, 0)$, then the eigenvectors of H_{RD} are written

$$\Psi_{RD\pm} = \frac{e^{i\mathbf{k}_{||}\cdot\mathbf{r}}}{2\pi\hbar}\frac{1}{\sqrt{2}} \begin{pmatrix} \mp\dfrac{-\lambda_D e^{i\theta} + i\lambda_R e^{-i\theta}}{\sqrt{\lambda_D^2 + \lambda_R^2 - 2\lambda_D\lambda_R \sin 2\theta}} \\ 1 \end{pmatrix} \tag{7}$$

In the pure Rashba case ($\lambda_D = 0$), the expectation value becomes

$$\langle\sigma\rangle_{R\pm} \propto \pm \begin{pmatrix} -\sin\theta \\ \cos\theta \\ 0 \end{pmatrix}. \tag{8}$$

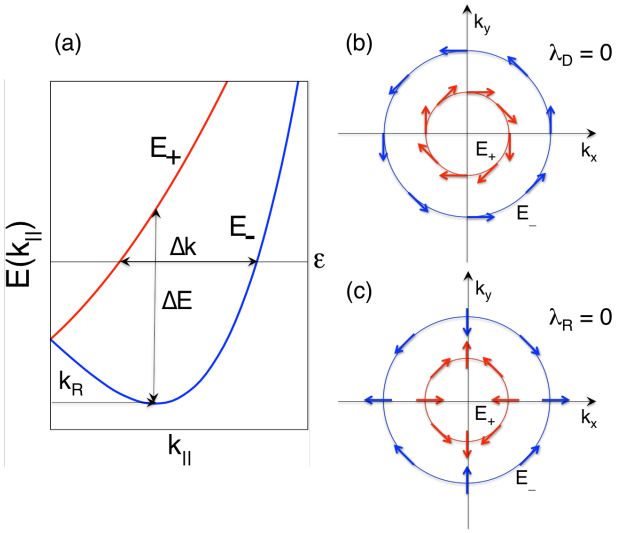

FIG. 1. (a) Dispersion for the inner (E_+, red line) and outer (E_-, blue line) branches for a C_{2v} system ruled by the Rashba-Dresselhaus Hamiltonian. The minimum momentum displacement is noted k_R and the amplitude of the splitting is noted ΔE. (b) Scheme of spin orientations for the corresponding eigenstates $\Psi_{RD\pm}$ in the case of pure Rashba effect (or SIA), *i.e.* $\lambda_D = 0$. (c) Same in the case of pure Dresselhaus Hamiltonian (or BIA), *i.e.* $\lambda_R = 0$.

We recover the well-known Rashba figure (Figure 1-b) with an in-plane orientation always orthogonal to the momenta direction. On the other hand, in the case of a pure Dresselhaus effect ($\lambda_R = 0$), then we write

$$\langle\sigma\rangle_{D\pm} \propto \pm \begin{pmatrix} \cos\theta \\ -\sin\theta \\ 0 \end{pmatrix},$$

which leads to very different spin textures (Figure 1-c) for the inner and outer branches characteristics of a BIA spin-splitting. The general case reads

$$\langle\sigma\rangle_{RD\pm} \propto \pm \begin{pmatrix} \lambda_D\cos\theta - \lambda_R\sin\theta \\ \lambda_D\sin\theta + \lambda_R\cos\theta \\ 0 \end{pmatrix}. \tag{9}$$

Thus, once $\langle\sigma\rangle_\pm$ is computed, One can deduce the relative strength of each effect. In the case of C_{2v} symmetry, even going to cubic terms the spin distribution remains in-plane. The situation is different with C_{3v} and D_{2d} symmetries where the Hamiltonian can contains cubic terms depending on σ_z. Then non-zero out-of-plane components of the spinors can occur.

The computational observation of the spin splittings is performed by computing the band structure around a high-symmetry point of the BZ. One has to be careful to properly define $\mathbf{k}_{||}$ based on the symmetry of the system. In addition, the spin texture is computed as well to identify and assess the existence and amplitude of Rashba and Dresselhaus effects. In the following, we conduct a survey on various hybrid organic-inorganic perovskites.

Rashba-type splittings have been designed and observed among QWs[22–25] and heterostructures[20,21] of classical semiconductors.[15] Hybrid organic-inorganic perovskites appear to be promising candidates in that respect thanks to the the giant SOC displayed.[9,10] Moreover, this family of compounds can be found in many different crystal structures. To conduct our survey we decided to start from the highly symmetrical $Pm\bar{3}m$ (n° 221) reference phase,[48] observed in the high temperature phase of numerous hybrid perovskites.[50–53] From this point we follow different phase transitions (Figure 2). A key point in the observation of a SOC induced spin-splitting is the loss of inversion symmetry. Therefore, we take interest in structures deprived of this particular symmetry such as ferroelectric structures. We consider 3D bulk examples belonging to $P4mm$ (n° 99), $R3m$ (n° 160) and $Amm2$ (n° 38) crystal groups. Then, we consider the case of a temperature induced ferroelectric transition in a bulk 2D perovskite. Finally, we consider an electric field induced phase transition. The latter structure presents inversion symmetry in $CH_3NH_3PbX_3$ compounds and should not be a suitable candidate for Rashba or Dresselhaus effect. Nevertheless, a controllable spin-splitting can be obtained with the application of an external electric field.

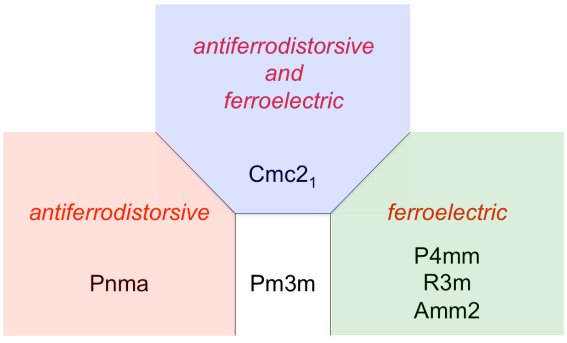

FIG. 2. Phase transitions from $Pm\bar{3}m$.

Halide organic-inorganic perovskites are hybrid materials and often show important distortions from the ideal octahedron. These deformations are in part responsible for the different properties of this class of perovskite.[54,55] However, if the loss of inversion symmetry

is a requirement for the spin-splitting, the loss of too many symmetry operations can lead to a unusable Rashba effect with uncharacteristic spin rotations.

NON-CENTROSYMMETRIC STRUCTURES

As a first case, we consider the methylammonium lead iodide perovskite $CH_3NH_3PbI_3$ in the $P4mm$ crystal group.[56] It corresponds to a simple translation of the ions along the z axis. The resulting structure shows a C_{4v} point group symmetry. The C_4 axis lies along the [001] crystallographic direction. Thus, [001] naturally defines the special quantization axis $\mathbf{k}_\perp$, $\mathbf{k}_{||}$ is contained in the plane that can be defined for instance by two vectors $\mathbf{k}_x$=[100] and $\mathbf{k}_y$=[010]. The critical point $\mathbf{k}_0$ is the point A (1/2,1/2,1/2). Figure 3-a displays the band structure of the $CH_3NH_3PbI_3$ calculated with and without SOC in the $\mathbf{k}_{||}$ plane. The SOC has three major contributions: (i) the gap is greatly reduced, (ii) the conduction band minimum (CBM) and the valence band maximum (VBM) are displaced away from A, (iii) the conduction and valence bands split away from A. The four resulting bands present similar spin textures (Figure 3-d) with spins orthogonal to the crystal momenta.

This pure Rashba picture is consistent with the predicted form of the spin-orbit Hamiltonian for a C_{4v} symmetry.[49] The apparent absence of deviation from the model (Figure 1-b) marks a weak or null contribution from cubic terms. From the momentum shift k_R and the energy splitting ΔE we calculate the strength of the Rashba effect $\lambda_R = \Delta E/(2k_R)$ and find a Rashba coefficient of $\lambda_R^{CBM} = 3.76$ eV.Å for the conduction band and $\lambda_R^{VBM} = 3.71$ eV.Å for the valence band. These Rashba splittings are on the same order as the largest splittings observed in bulk materials, e.g. $\lambda_R = 3.80$ eV.Å for BiTeI,[26] or surface alloys, e.g. $\lambda_R = 3.05$ eV.Å for Bi/Ag(111).[30]

From the $Pm\bar{3}m$ reference structure simultaneous translations of the ions along the three crystallographic axes lead to a $R3m$ structure. The corresponding point group symmetry is C_{3v}. In the case of methylammonium germanium iodide $CH_3NH_3GeI_3$,[56] the C_3 quantization axis ($\mathbf{k}_\perp$) is parallel to the [111] crystallographic direction. Hence, the relevant plan to observe a Rashba-like spin-splitting ($\mathbf{k}_{||}$) contains the directions [1-10] and [11-2] directions. In Figure 3-b, we plot the band structure following the relevant path around the critical point L (-1/2,1/2,1/2). The splitting is observed for both conduction and valence bands. The effect appears more pronounced in the conduction band. The spin textures (Figure 3-e) are again

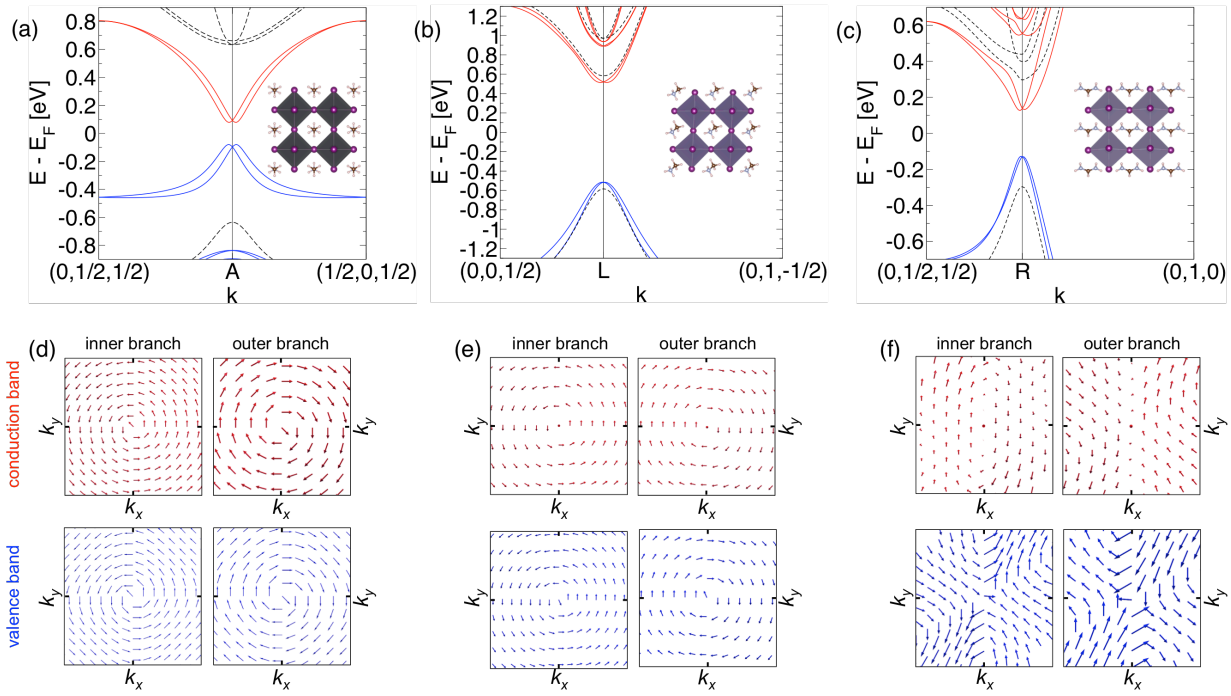

FIG. 3. Hybrid organic-inorganic halide perovskites crystallized in phases corresponding to a ferroelectric phase transition. (a) Band structure and structure (insert) for $CH_3NH_3PbI_3$ in the *P4mm* phase. Blue and red lines stand for the occupied and unoccupied bands for a calculation including SOC, respectively. Black dashed lines are the results of calculations without SOC. (b) Same for $CH_3NH_3GeI_3$ in a *R3m* structure. (c) Same for $CH(NH_2)_2SnI_3$ crystallized in the *Amm2* group. (d), (e) and (f) Spin textures for the inner and outer branches for both occupied and unoccupied bands for $CH_3NH_3PbI_3$, $CH_3NH_3GeI_3$ and $CH(NH_2)_2SnI_3$, respectively.

characteristic of a pure Rashba spin-splitting as predicted by the symmetry reduction of the $k \cdot p$ Hamiltonian in the case of a C_{3v} point group.[49] As in the case of $CH_3NH_3PbI_3$, there is no measurable out-of-plane component of the spin vectors. We extract again the values of λ_R and find $\lambda_R^{CBM} = 0.89$ eV.Å, $\lambda_R^{VBM} = 0.45$ eV.Å. These values are much weaker than in the case of $CH_3NH_3PbI_3$. The lowering of the Rashba spin splitting is expected as the atomic SOC splitting is much less important for the Pb^{2+} ion than for Ge^{2+} (1.75 *vs.* 0.22 eV).

$CH_3NH_3GeCl_3$ also crystallizes in a *R3m* structure.[52] With chlorine, the structure is more distorted than in the case of iodine (Figure S1-a in Supporting Information). The band structure remains similar with a band splitting in conduction and valence bands (Figure S1-b). The difference is quantitative with $\lambda_R^{CBM} = 1.18$ eV.Å and $\lambda_R^{VBM} = 0.23$ eV.Å. The

Rashba effect appears stronger in the conduction band than in the case of $CH_3NH_3GeI_3$. The Rashba effect is thus resilient to important lattice distortions. However, the spin textures show, in addition to the expected shape, important out-of-plane components even for small values of the momentum (Figure S1-c and d). This strain-induced alteration of electronic eigenvectors is a detrimental effect that may hinder the definition of purely intricated spin states for device applications (vide infra).

As a final example of ferroelectric structures we study the case of $CH(NH_2)_2SnI_3$ in the $Amm2$ group.[45,57] It corresponds to twin translations of the ions along the x and y directions The resulting point group symmetry is C_{2v}, with the C_2 axis in the [011] direction. We plot the band structure around R (1/2,1/2,1/2) probing the [100] and [01-1] directions. The splitting of bands occurs for both the conduction and valence bands. However, the spin textures close to the CBM and VBM for the inner and outer branches (Figure 3-f) are very different from the previous examples even if no out-of-plane contribution is noted. It does not correspond to any limit cases presented Figure 1. As detailed previously, a system in the C_{2v} symmetry can exhibit both Rashba and Dresselhaus terms (Eq. 2). Using Eq., 9 and the spin orientations for different momentum, we get the relative contributions of both effects being $\lambda_D^{CBM} = 2.59$ eV.Å and $\lambda_R^{CBM} = 0.50$ eV.Å. Our results are in good agreement with previous GW calculations (where the Rashba and Dresselhaus parameters are computed as $\Delta E/k_R$, accounting for the factor 2 discrepancy between their and our results).[45] The effect is too weak in the valence band and no parameter can be computationally assessed in this case.

FERROELECTRIC TRANSITIONS: TEMPERATURE-CONTROLLED RASHBA SPIN-SPLITTING

The ideal reference structure for bulk 2D hybrid perovskites corresponds to a D_{4h} point group symmetry.[58] High temperature centrosymmetric crystal phases of 2D hybrid perovskites however usually exhibit a cell doubling in a plane perpendicular to the stacking axis, associated to antiferrodistorsive tilts of the octahedra. This lattice distortion leads to a reduction of the point group symmetry from D_{4h} to D_{2h} and a BZ folding from the M point at the BZ boundary to the Γ point at the BZ center. Such a structure is observed at high temperature for the 2D hybrid perovskite Bz_2PbI_4 (Bz = benzylammonium)[59,60] which

crystallizes in a $Cmca$ (n° 64) centrosymmetric phase.[60] The structure is layered with slabs of single octahedrons sandwiched by slabs of organic cations (Figure 4). The crystal undergoes below T = 438 K a ferroelectric phase transition to a $Cmc2_1$ non-centrosymmetric structure.

The C_2 quantization axis in the low temperature phase is along the [001] crystallographic direction and thus no spin-splitting occurs on the $\Gamma \rightarrow Z$ path (Figure 4-a). Following the previous scheme, $\mathbf{k}_{||}$ should be defined by [100] and [001]. As, [100] correspond to the stacking direction, there is no dispersion of the bands due to the inorganic part in that direction.[9] The spin-splitting can be observed following $\Gamma \rightarrow X$. This situation notably differs from the Rashba effect in conventional semiconductor QW and heterostructures, where the stacking and quantization axes coincide. Therefore, the problem becomes analog to a 1D problem with contributions involving only k_y:

$$\mathcal{H}(\mathbf{k}_x) = -\lambda_R k_y \sigma_x + \lambda_D k_y \sigma_y.$$

The eigenvalues and eigenvectors become

$$E_{RD\pm}(k_y) = \frac{\hbar k_y^2}{2m} \pm \sqrt{(\lambda_D^2 + \lambda_R^2) k_y^2}$$

$$\Psi_{1D\pm} \propto \begin{pmatrix} \mp \dfrac{\lambda_R - i\lambda_D}{\sqrt{\lambda_R^2 + \lambda_D^2}} \dfrac{k_y}{|k_y|} \\ 1 \end{pmatrix},$$

and the spin textures

$$\langle \sigma \rangle_{\pm} \propto \begin{pmatrix} \mp \dfrac{k_y}{|k_y|} \\ 0 \\ 0 \end{pmatrix}.$$

Only one spin component is obtained along the stacking direction. Clearly, there is no differential impact on the observables (band splitting and σ expectation values) of the nature Rashba *vs.* Dresselhaus of the spin splitting. Then, one can note λ the effective amplitude given by

$$\lambda = \frac{\Delta E_{RD}(k_y)}{2k_y}.$$

The band structure calculated for a low-temperature structure (93 K) of Bz_2PbI_4 (Figure 4-a) shows a large effect on the conduction band ($\lambda^{CBM} = 2.14$ eV.Å) and much weaker

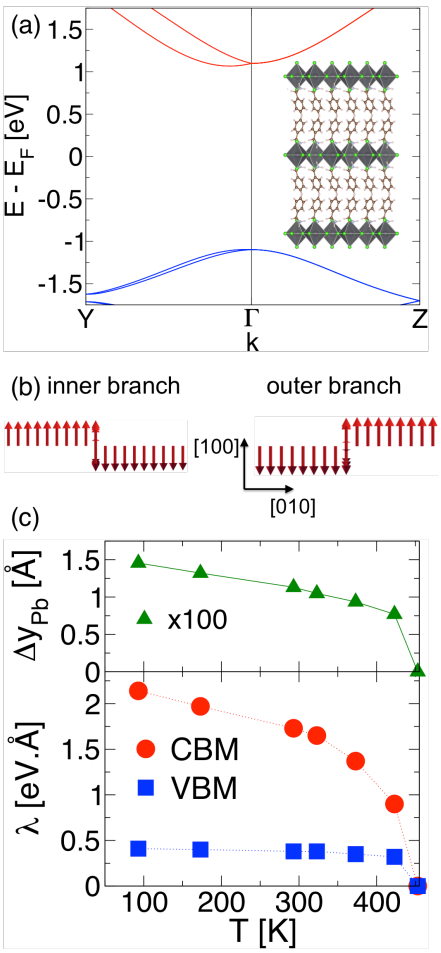

FIG. 4. (a) Band structure of Bz_2PbI_4 in the low temperature $Cmc2_1$ phase, computed with SOC. Blue and red bands correspond to occupied and unoccupied band, respectively. (b) Spin textures for the inner and outer branches of the conduction band. (c) Temperature dependance of the Pb displacement along y (see text) and computed Rashba parameters for the conduction and valence band.[60]

on the valence band ($\lambda^{VBM} = 0.41$ eV.Å). The spin textures for both branches of the conduction band (Figure 4-b) display the expected figure with a single component whatever the momentum.

Recently, Liao *et al.* have characterized the crystal structure of Bz_2PbI_4 at various temperatures.[60] The crystal remains in the $Cmc2_1$ group for temperatures from 93 K up to 423 K. The high temperature structure (453K) presents a $Cmca$ symmetry, *i.e.* a D_{2h} point group symmetry and, therefore, does not exhibit spin-splitting. We compute the electronic structure for each structure and determine the evolution of the Rashba parameter λ with

temperature (Figure 4-c). The temperature induced variation of the Rashba parameter can be related to the order parameter of the $Cmca$ (D_{2h}) to $Cmc2_1$ (C_{2v}) ferroelectric phase transition. This order parameter corresponds to the $B1u$ irreducible representation (IR) of the D_{2h} point group and to a polarization along the C2 axis ([001] direction). The analysis of the $Cmca$ phonons modes shows that the $B1u$ IR appears both in the mechanical representations of the Pb and Cl atoms, with a parallel motions of two Pb (or Cl) atoms along the z axis and antiparallel motions along the y axis. The low temperature $Cmc2_1$ phase can thus be partly described as a displacive distortion from the $Cmca$ phase with the corresponding atomic displacements from their high temperature positions. We shall point out that the phase transition is also related to an order-disorder character in relation with the disordered orientations of the organic molecules in the $Cmca$ phase. The splitting in the valence band is weakly affected by the structural changes occurring from 93 to 423 K with a λ^{VBM} slowly varying from 0.41 eV.Å to 0.32 eV.Å. On the other hand, the Rashba effect in the conduction bands is stronger This smooth variation is related to the atomic displacement in the low temperature phase. Indeed, the decrease from 2.14 eV.Å to 0.90 eV.Å can be traced back to structural characteristics such as the displacement of Pb atoms along y (Figure 4 and S2 and S3).

The effect of octahedron distortions ($CH_3NH_3GeCl_3$) and of the in-plane and out-of-plane tilts (Bz_2PbI_4) have illustrated the delicate balance of symmetry/asymmetry required to observe a Rashba effect in materials. In the following, we consider the case of a spin-splitting ruled by an external electric field.

FIELD-CONTROLLED RASHBA SPIN-SPLITTING

We propose in this part to use an electric fiel-controlled Rashba splitting starting from 3D hybrid perovskites. An electric field applied to the $Pm\bar{3}m$ reference structure correspond to a Γ^{4-} perturbation, and may lead to one of the three ferroelectric distortion already described in the first part. The organic cations are however dynamically disordered in the $Pm\bar{3}m$ phase, and we rather propose a DFT simulation of this effect in the low-temperature $Pnma$ antiferrodistorsive distortion of the $Pm\bar{3}m$ phase. This centrosymmetric structure is often encountered among hybrid organic-inorganic perovskite[52,53,61] and is, in particular, the low-temperature phase of $CH_3NH_3PbI_3$,[61] the most used perovskite in recent developments

in photovoltaics. The *Pnma* crystal group corresponds to a D_{2h} point group symmetry and presents inversion symmetry. Therefore, no Rashba effect can be expected in this case. Nevertheless, when a transverse external electric eld $\mathbf{E}_{\text{ext}}$ is applied, the inversion symmetry is lost and a spin splitting is expected.

The control of spin splitting, and thus of the Rashba parameter, by a gate voltage, *i.e.* an external electric field, has been under intense investigation ever since the mid-1990s.[21–23,31] In the early 2000s, theoretical works have help rationalized the effect. In particular, tight-binding models have provided with the essential tools to evaluate the Rashba parameter as a function of microscopic quantities.[15,62–65] Recently, Kim and coworkers have adapted the model to hybrid organic-inorganic perovskites in the case of non-centrosymmetric structures without an external electric field.[43] The complete description of those models is out of the scope of this work, let us recall here that they describe a Rashba parameter that depends linearly on the atomic SOC and on the effective potential gradient but decreases when the gap increases.

In order to apply the electric field, we start from the bulk structure of $CH_3NH_3PbI_3$ in the *Pnma* phase, and construct slabs terminated by the [010] surface, containing n_{cell} octahedrons in the packing direction. Two cases occur: (i) n_{cell} is even (Figure 5-a) then the resulting structure belongs to the non-centrosymmetric group $Pmc2_1$ (n° 26) corresponding to the C_{2v} point group, (ii) n_{cell} is odd (Figure 5-e), then the structure presents a $P2_1/c$ (n° 14) group symmetry with inversion symmetry (C_{2h} point group). The consequence of this odd/even difference can be seen in the band structures calculated for slabs with n_{cell} = 2 and 3 (Figure 5-b and f) around Γ in both in-plane directions [100] and [010]. Indeed, no splitting is observed for the conduction and valence bands of the system with n_{cell} = 3, whereas for n_{cell} = 2, a small splitting can be seen in the Γ → X (1/2,0,0) direction. However, this is not the case when going to thicker slabs: for slabs with n_{cell} = 4 and more, no splitting is retrieved in our calculations.

A spin splitting is observed when applying a transverse electric field $\mathbf{E}_{\text{ext}}$ (Figure 5-c and g). This effect is almost null in the conduction band but can lead to amplitudes λ of nearly 0.5 eV.Å in the valence band. Whatever the thickness of the slab, bands close to the gap are not surface states and the splitting is not a difference between up and down faces of the slab. The spin textures of the inner and outer branches of the valence band are similar for odd and even cases (Figure 5-d and h) and correspond to a Rashba spin splitting.

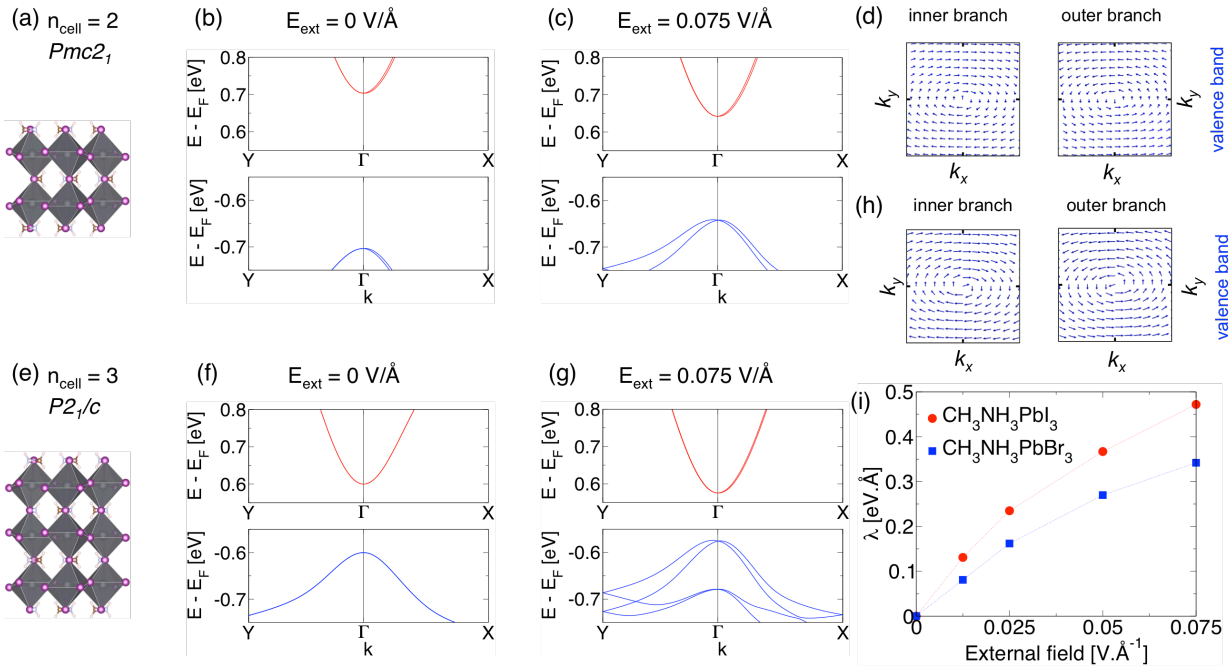

FIG. 5. Electric field induced spin-splitting in slabs of $CH_3NH_3PbI_3$. The original bulk crystal group is *Pnma*. Slabs with even and odd thickness (n_{cell}) exhibit $Pmc2_1$ and $P2_1/c$ symmetry, respectively. (a) and (e) Structures of slabs of $CH_3NH_3PbI_3$ with $n_{cell} = 2$ and 3. Pb, I, N, C and H are depicted in gray, purple, blue, brown and white, respectively. (b) and (f) Corresponding band structure computed with SOC. Blue and red bands correspond to occupied and unoccupied band, respectively. A small splitting is observed in the case of $n_{cell} = 2$. (c) and (g) Same with the application of an external electric field $E_{ext} = 0.075$ VÅ^{-1}. A splitting is observed with corresponding spin textures depicted in (d) and (h) for the valence bands. (i) Rashba parameter λ (eV.Å) as a function of the applied electric field E_{ext} (VÅ^{-1}) for $CH_3NH_3PbI_3$ (red circles) and $CH_3NH_3PbBr_3$ (blue squares).

We monitor the evolution of the valence band Rashba parameter λ with the amplitude of the applied transverse electric field E_{ext} (Figure 5-i). Let us note that for $n_{cell} \geq 7$, the bulk gap is recovered and the Rashba parameter ceases to depend on the thickness of the slab (Figure S3.). That is to say, a bulk-like behavior is described. λ owes its increase to two electric field effects: (i) the induced asymmetry, (ii) to the band gap modulation due to the Stark effect that tends to close the gap. We observe a linear dependance of λ with respect to the external field E_{ext} for weak fields. In addition to the external field, the amplitude of the Rashba parameter is affected by the atomic SOC and by the original (no field) band gap of

the materials. This can be verified by applying the same procedure to $CH_3NH_3PbBr_3$ in the same *Pnma* phase.[66] This way the atomic SOC is almost constant and only the band gap is modified. It varies from 1.03 eV for $CH_3NH_3PbI_3$ to 1.38 eV for $CH_3NH_3PbBr_3$ in our DFT+SOC calculations, whose underestimation of semiconductor band gaps is well-known. We find a 28% diminution of λ going from I to Br that is in correct agreement with the 33% increase of the band gap. When the field becomes stronger, a bending is observed that might be the manifestation of higher orders terms.

The aspiration for a field-controlled Rashba spin-splitting was first motivated by the design of a spin FET following the original scheme proposed by Datta and Das in 1990 (Figure 6).[67] In this setup, the electron spins precess under the influence of the Rashba and/or Dresselhaus coupling. Then, by tuning the amplitude of the effect, one will act on the phase and the electron leaving the source can reach the drain in or out-of-phase. After the very first observations of tunable Rashba splitting,[21–23] several examples of devices have been produced[37,38,68,69] or proposed on the base of theoretical inspections.[70,71] More elaborated devices have been proposed based on the same principle, adding a transverse magnetic field to the electric one and the use of more than one site for SOC effect. In this manner a perfect spin filter can be achieved.[72–74]

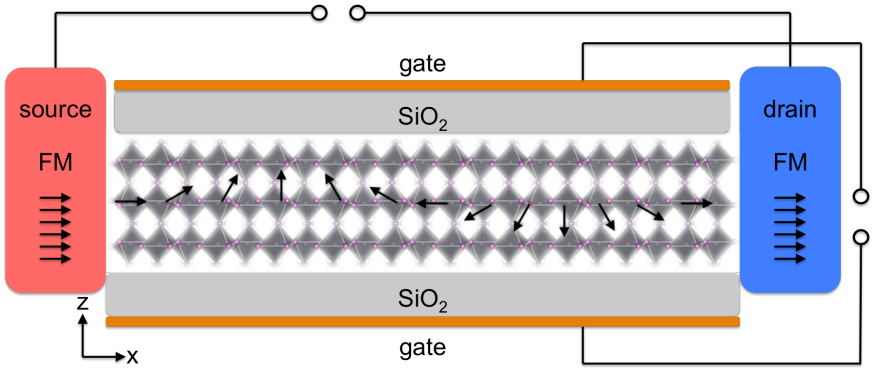

FIG. 6. Scheme of a sFET as proposed by Datta and Das[67] based on hybrid organic-inorganic perovskites with a representation of the spin precession from the source to the drain.

Based on our findings, a similar scheme can be proposed based on the low cost hybrid organic-inorganic perovskite $CH_3NH_3PbI_3$, in the *Pnma* structure. Contrary to the previous examples, the suggested setup presents no manifestation of the SOC when the electric field is null ($\lambda = 0$ eV.Å) which makes less delicate the tuning of the source-drain distance and of the amplitude of the transverse field E_{ext}.

Let us consider the case of a ferromagnetic source and drain with magnetizations along $+x$ being also the direction of propagation of the electron. In the semiconductor part of the transistor we find the quantization axis along z, which is the orientation of the gate. The electron is injected with a magnetization along x, *i.e.* presents a spinor of the form $1/\sqrt{2}(1,1)$, with an energy ϵ. In the case of a Rashba spin-splitting, from Eq. 7, the basis on which the spinors are then decomposed is then given by

$$|+\rangle = \frac{1}{\sqrt{2}}\begin{pmatrix} -i \\ 1 \end{pmatrix}, \text{ and } |-\rangle = \frac{1}{\sqrt{2}}.\begin{pmatrix} +i \\ 1 \end{pmatrix}$$

The $+x$ oriented spin is then expressed as

$$|+x\rangle = \frac{1}{2}\Big[(1+i)|+\rangle + (1-i)|-\rangle\Big].$$

$|+\rangle$ and $|-\rangle$ eigenstates propagate with momentum k_+ and k_- given by Eq. , with

$$\Delta k = k_- - k_+ = \frac{2m}{\hbar^2}\lambda_R$$

and the wavefunction of the propagating electron is given by

$$\Psi(x) = \frac{1}{2}\left[(1+i)\frac{e^{ik_+x}}{\sqrt{2}}\begin{pmatrix} -i \\ 1 \end{pmatrix} + (1-i)\frac{e^{ik_-x}}{\sqrt{2}}\begin{pmatrix} +i \\ 1 \end{pmatrix}\right]$$

and the expectation value $\langle\sigma\rangle$ at the distance L is

$$\langle\sigma\rangle \propto \begin{pmatrix} \cos(\Delta k.L) \\ 0 \\ -\sin(\Delta k.L) \end{pmatrix}.$$

One can see that the spin precesses in the (x,z) plane. To obtain a spin anti-align (off-state) with the magnetization of the drain (Figure 6), the length should be tuned such as

$$\Delta k.L_{\text{off}} = (n+\frac{1}{2})\pi,$$

where n is an integer. And thus,

$$L_{\text{off}} = (n+\frac{1}{2})\frac{\pi\hbar^2}{m\lambda_R}.$$

If we consider a device with a thickness of 10 nm, then an applied field of 0.0125 V.Å corresponds to a gate voltage of 1.25 V and a λ_R of around 0.1 eV.Å. Then, the lengths corresponding to off-states are 12 nm ($n=0$), 36 nm ($n=1$), etc.

CONCLUSION

Hybrid inorganic-organic perovskite have become extremely popular over the last five years, in the field of photovoltaics. In this respect, they were initially regarded as dyes and, as such, related to oragnometallics dyes. However, these materials were first considered, in the 2D form, for applications in optoelectronics, and related to classical semiconductors. Here we pursue the filiation with the world of semiconductors and conduct a survey of the Rashba and Dresselhaus effects in these atypical semiconductor. We have recalled the general conditions to observe a Rashba and Dresselhaus spin splittings based on symmetry analysis and $\mathbf{k} \cdot \mathbf{p}$ expansion. We apply this approach to several examples in non-centrosymmetric structures presenting C_{4v}, C_{3v} and C_{2v} symmetries. Even for Ge-based compounds we find Rashba parameters of nearly 1 eV.Å. Proving that despite the important distortions caused by the organic cation, the SOC effect prevails. In an example of 2D non-centrosymmetric structure we can monitor the amplitude of the splitting with respect to the temperature due to the continuous polarization of the crystal structure from high to low temperature. Finally we inspect the case of centrosymmetric structure exhibiting a Rashba spin splitting under the influence of a transverse electric field. The possibility to control the spin precession in the material thanks to a gate voltage constitutes the base for a hybrid organic-inorganic perovskite-based spin FET.

COMPUTATIONAL DETAILS

First-principles calculations are based on DFT as implemented in the SIESTA package.[75,76] Calculations have been carried out with the GGA functional in the PBE form,[77] Troullier-Martins pseudopotentials,[78] and a basis set of finite-range numerical pseudoatomic orbitals for the valence wave functions.[79] Structures relaxation and electronic structure calculations have been done using a double-ζ polarized basis sets.[79] In our calculations, SOC is taken into account through the on-site approximation as proposed by Fernández-Seivane *et al.*[80] In all cases, an energy cutoff of 150 Ry for real-space mesh size has been used. In the case of $CH_3NH_3PbI_3$ and $CH_3NH_3PbBr_3$ slabs, the bulk has been relaxed, but no subsequent geometry relaxation has been conducted on slabs. This strategy allows us to stay as close as possible from the bulk behavior of the materials.

We have repeated selected calculations using plane wave basis sets and the projected augmented wave method as implemented in VASP.[81,82] We have used the same structures relaxed by SIESTA with the same exchange and correlation scheme and k-points sampling. The cutoff energy has been chosen between 300 and 500 eV depending on the structure. The results obtained with VASP confirm the main features previously obtained by SIESTA. We have also used the VASP results to plot the spin textures.

---

* mikael.kepenekian@univ-rennes1.fr

† jacky.even@insa-rennes.fr

[1] A. Kojima, K. Teshima, Y. Shirai, and T. Miyasaka, J. Am. Chem. Soc. **131**, 6050 (2009).

[2] H. J. Snaith, J. Phys. Chem. Lett. **4**, 3623 (2013).

[3] M. A. Green, A. Ho-Baillie, and H. J. Snaith, Nature Photon. **8**, 506 (2014).

[4] M. Grätzel, Nature Mater. **13**, 838 (2014).

[5] H. Zhou, Q. Chen, G. Li, S. Luo, T. Song, H.-S. Duan, Z. Hong, J. You, Y. Liu, and Y. Yang, Science **345**, 542 (2014).

[6] D. B. Mitzi, C. A. Feild, W. T. A. Harrison, and A. M. Guloy, Nature **369**, 467 (1994).

[7] D. B. Mitzi, S. Wang, C. A. Feild, C. A. Chess, and A. M. Guloy, Science **267**, 1473 (1995).

[8] C. R. Kagan, D. B. Mitzi, and C. D. Dimitrakopoulos, Science **286**, 945 (1999).

[9] J. Even, L. Pedesseau, M.-A. Dupertuis, J.-M. Jancu, and C. Katan, Phys. Rev. B **86**, 205301 (2012).

[10] J. Even, L. Pedesseau, J.-M. Jancu, and C. Katan, J. Phys. Chem. Lett. **4**, 2999 (2013).

[11] J. Even, L. Pedesseau, J.-M. Jancu, and C. Katan, Phys. Status Solidi RRL **8**, 31 (2014).

[12] G. Dresselhaus, Phys. Rev. **100**, 580 (1955).

[13] E. I. Rashba, Sov. Phys. Solid State **2**, 1224 (1960).

[14] Y. A. Bychkov and E. I. Rashba, JETP Lett. **39**, 78 (1984).

[15] R. Winkler, *Spin-Orbit Coupling Effects in Two-Dimensional Electron and Hole Systems* (Springer, 2003).

[16] J. H. Dil, J. Phys.: Condens. Matter **21**, 403001 (2009).

[17] S. D. Ganichev and L. E. Golub, phys. stat. sol. (b) **251**, 1801 (2014).

[18] X. Zhang, Q. Liu, J.-W. Luo, A. J. Freeman, and A. Zunger, Nature Phys. **10**, 387 (2014).

[19] G. Bihlmayer, O. Rader, and R. Winkler, New J. Phys. **17**, 050202 (2015).

[20] G. Lommer, F. Malcher, and U. Rossler, Phys. Rev. Lett. **60**, 728 (1988).

[21] J. Nitta, T. Akazaki, H. Takayanagi, and T. Enoki, Phys. Rev. Lett. **78**, 1335 (1997).

[22] M. Schultz, F. Heinrichs, U. Merkt, T. Colin, T. Skauli, and S. Løvold, Semicond. Sci. Technol. **11**, 1168 (1996).

[23] G. Engels, J. Lange, T. Schäpers, and H. Lüth, Phys. Rev. B **55**, R1958 (1997).

[24] A. Balocchi, T. Amand, G. Wang, B. L. Liu, P. Renucci, Q. H. Duong, and X. Marie, New J. Phys. **15**, 095016 (2013).

[25] G. Wang, A. Balocchi, A. V. Poshakinskiy, C. R. Zhu, S. A. Tarasenko, T. Amand, B. L. Liu, and X. Marie, New J. Phys. **16**, 045008 (2014).

[26] K. Ishizaka, M. S. Bahramy, H. Murakawa, M. Sakano, T. Shimojima, T. Sonobe, K. Koizumi, S. Shin, H. Miyahara, A. Kimura, K. Miyamoto, T. Okuda, H. Namatame, M. Taniguchi, R. Arita, N. Nagaosa, K. Kobayashi, Y. Murakami, R. Kumai, Y. Kaneko, Y. Onose, and Y. Tokura, Nature Mater. **10**, 521 (2011).

[27] T. Ideue, J. G. Checkelsky, M. S. Bahramy, H. Murakawa, Y. Kaneko, N. Nagaosa, and Y. Tokura, Phys. Rev. B **90**, 161107(R) (2014).

[28] S. LaShell, B. A. McDougall, and E. Jensen, Phys. Rev. Lett. **77**, 3419 (1996).

[29] Y. M. Koroteev, G. Bihlmayer, J. E. Gayone, E. V. Chulkov, S. Blügel, P. M. Echenique, and P. Hofmann, Phys. Rev. Lett. **93**, 046403 (2004).

[30] C. R. Ast, J. Henk, A. Ernst, L. Moreschini, M. C. Falub, D. Pacilé, P. Bruno, K. Kern, and M. Grioni, Phys. Rev. Lett. **98**, 186807 (2007).

[31] A. Takayama, T. Sato, S. Souma, T. Oguchi, and T. Takahashi, Nano Lett. **12**, 1776 (2012).

[32] M. Bianchi, R. C. Hatch, Z. Li, P. Hofmann, F. Song, J. Mi, B. B. Iversen, M. Abd El-Fattah, P. Löptien, L. Zhou, A. A. Khajetoorians, J. Wiebe, R. Wiesendanger, and J. W. Wells, ACS Nano **6**, 7009 (2012).

[33] S. V. Eremeev, I. P. Rusinov, I. A. Nechaev, and E. V. Chulkov, New J. Phys. **15**, 075015 (2013).

[34] A. F. Santander-Syro, F. Fortuna, C. Bareille, T. C. Rödel, G. Landolt, N. C. Plumb, J. H. Dil, and M. Radović, Nature Mater. **13**, 1085 (2014).

[35] E. Wang, P. Tang, G. Wan, A. V. Fedorov, I. Miotkowski, Y. P. Chen, W. Duan, and S. Zhou, Nano Lett. **15**, 2031 (2015).

[36] A. Banerjee, F. Dogan, J. Heo, A. Manchon, W. Guo, and P. Bhattacharya, Nano Lett. **11**, 5396 (2011).

[37] D. Liang and X. P. A. Gao, Nano Lett. **12**, 3263 (2012).

[38] S. Zhang, N. Tang, W. Jin, J. Duan, X. He, X. Rong, C. He, L. Zhang, X. Qin, L. Dai, Y. Chen, W. Ge, and B. Shen, Nano Lett. **15**, 1152 (2015).

[39] J. F. Gregg, I. Petej, E. Jouguelet, and C. Dennis, J. Phys. D: Appl. Phys. **35**, R121 (2002).

[40] R. Jansen, J. Phys. D: Appl. Phys. **36**, R289 (2003).

[41] I. Zutić, J. Fabian, and S. Das Sarma, Rev. Mod. Phys. **76**, 323 (2004).

[42] R. Jansen, Nature Mater. **11**, 400 (2012).

[43] M. Kim, J. Im, A. J. Freeman, J. Ihm, and H. Jin, Proc. Natl. Acad. Sci. U.S.A. **111**, 6900 (2014).

[44] F. Brivio, K. T. Butler, A. Walsh, and M. van Schilfgaarde, Phys. Rev. B **89**, 155204 (2014).

[45] A. Stroppa, D. Di Sante, P. Barone, M. Bokdam, G. Kresse, C. Franchini, M.-H. Whangbo, and S. Picozzi, Nature Commun. **5**, 5900 (2014).

[46] Y. Kutes, L. Ye, Y. Zhou, S. Pang, B. D. Huey, and N. P. Padture, J. Phys. Chem. Lett. **5**, 3335 (2014).

[47] D. Giovanni, H. Ma, J. Chua, M. Grätzel, R. Ramesh, S. Mhaisalkar, N. Mathews, and T. C. Sum, Nano Lett. **15**, 1553 (2015).

[48] J. Even, J. Phys. Chem. Lett. **6**, 2238 (2015).

[49] S. Vajna, E. Simon, A. Szilva, K. Palotas, B. Ujfalussy, and L. Szunyogh, Phys. Rev. B **85**, 075404 (2012).

[50] A. Poglitsch and D. Weber, J. Chem. Phys. **87**, 6373 (1987).

[51] K. Yamada, Y. Kuranaga, K. Ueda, S. Goto, T. Okuda, and Y. Furukawa, Bull. Chem. Soc. Jpn. **71**, 127 (1998).

[52] K. Yamada, K. Mikawa, T. Okuda, and K. S. Knight, Dalton Trans. , 2112 (2002).

[53] L. Chi, I. Swainson, L. Cranswick, J.-H. Her, P. Stephens, and O. Knop, J. Solid State Chem. **178**, 1376 (2005).

[54] M. R. Filip, G. E. Eperon, H. J. Snaith, and F. Giustino, Nat. Commun. **5**, 5757 (2014).

[55] C. Katan, L. Pedesseau, M. Kepenekian, A. Rolland, and J. Even, J. Mater. Chem. A **3**, 9232 (2015).

[56] C. C. Stoumpos, L. Frazer, D. J. Clark, Y. S. Kim, S. H. Rhim, A. J. Freeman, J. B. Ketterson,

J. I. Jang, and M. G. Kanatzidis, J. Am. Chem. Soc. **137**, 6804 (2015).

[57] C. C. Stoumpos, C. D. Malliakas, and M. G. Kanatzidis, Inorg. Chem. **52**, 9019 (2013).

[58] J. L. Knutson, J. D. Martin, and D. B. Mitzi, Inorg. Chem. **44**, 4699 (2005).

[59] M. Braun and W. Frey, Z. Kristallogr. New Cryst. Struct. **214**, 331 (1999).

[60] W.-Q. Liao, Y. Zhang, C.-L. Hu, J.-G. Mao, H.-Y. Ye, P.-F. Li, S. D. Huang, and R.-G. Xiong, Nat. Commun. **6**, 7338 (2015).

[61] T. Baikie, Y. Fang, J. M. Kadro, M. Schreyer, F. Wei, S. G. Mhaisalkar, M. Grätzel, and T. J. White, J. Mater. Chem. A **1**, 5628 (2013).

[62] L. Petersen and Hedegård, Surf. Sci. **459**, 49 (2000).

[63] C. L. Kane and E. J. Mele, Phys. Rev. Lett. **95**, 226801 (2005).

[64] S. Konschuh, M. Gmitra, and J. Fabian, Phys. Rev. B **82**, 245412 (2010).

[65] C. R. Ast and I. Gierz, Phys. Rev. B **86**, 085105 (2012).

[66] I. P. Swainson, R. P. Hammond, C. Soullière, O. Knop, and W. Massa, J. Solid State Chem. **176**, 97 (2003).

[67] S. Datta and B. Das, Appl. Phys. Lett. **56**, 665 (1990).

[68] C. Yin, H. Yuan, X. Wang, S. Liu, S. Zhang, N. Tang, F. Xu, Z. Chen, H. Shimotani, Y. Iwasa, Y. Chen, W. Ge, and B. Shen, Nano Lett. **13**, 2024 (2013).

[69] K.-H. Kim, D.-S. Um, H. Lee, S. Lim, J. Chang, H. C. Koo, M.-W. Oh, H. Ko, and H. Kim, ACS Nano **7**, 9106 (2013).

[70] D. Di Sante, P. Barone, R. Bertacco, and S. Picozzi, Adv. Mater. **25**, 509 (2013).

[71] Q. Liu, Y. Guo, and A. J. Freeman, Nano Lett. **13**, 5264 (2013).

[72] R. Citro, F. Romeo, and M. Marinaro, Phys. Rev. B **74**, 115329 (2006).

[73] A. Aharony, Y. Tokura, G. Z. Cohen, O. Entin-Wohlman, and S. Katsumoto, Phys. Rev. B **84**, 035323 (2011).

[74] S. Matityahu, A. Aharony, O. Entin-Wohlman, and S. Tarucha, New J. Phys. **15**, 125017 (2013).

[75] J. M. Soler, E. Artacho, J. D. Gale, A. García, J. Junquera, P. Ordejón, and D. Sánchez-Portal, J. Phys.: Condens. Matter **14**, 2745 (2002).

[76] E. Artacho, E. Anglada, O. Diéguez, J. D. Gale, A. García, J. Junquera, R. M. Martin, P. Ordejón, J. M. Pruneda, D. Sánchez-Portal, and J. M. Soler, J. Phys.: Condens. Matter **20**, 064208 (2008).

[77] J. P. Perdew, K. Burke, and M. Ernzerhof, Phys. Rev. Lett. **77**, 3865 (1996).

[78] N. Troullier and J. L. Martins, Phys. Rev. B **43**, 1993 (1991).

[79] E. Artacho, D. Sánchez-Portal, P. Ordejón, A. García, and J. M. Soler, phys. stat. sol. (b) **215**, 809 (1999).

[80] L. Fernández-Seivane, M. A. Oliveira, S. Sanvito, and J. Ferrer, J. Phys.: Condens. Matter **18**, 7999 (2006).

[81] G. Kresse and J. Furthmüller, Comput. Mat. Sci. **6**, 15 (1996).

[82] G. Kresse and J. Furthmüller, Phys. Rev. B **54**, 11169 (1996).